

First Measurement of a Weak r -Process Reaction on a Radioactive Nucleus

M. Williams^{1,*} C. Angus^{2,3} A. M. Laird^{3,2} B. Davids^{2,4} C. Aa. Diget^{3,2} A. Fernandez⁵ E. J. Williams²
 A. N. Andreyev³ H. Asch⁴ A. A. Avaa² G. Bartram¹ S. Chakraborty^{2,3} I. Dillmann² K. Directo²
 D. T. Doherty¹ E. Geerlof² C. J. Griffin² A. Grimes² G. Hackman² J. Henderson¹ K. Hudson^{4,2} D. Hufschmidt⁵
 J. Jeong^{6,2} M. C. Jiménez de Haro⁵ V. Karayonchev^{2,†} A. Katrusiak² A. Lennarz^{2,7} G. Lotay¹ B. Marlow²
 M. S. Martin^{4,‡} S. Molló^{8,2} F. Montes⁹ J. R. Murias² J. O'Neill¹ K. Pak^{6,2} C. Paxman^{1,§} L. Pedro-Botet^{8,2}
 A. Psaltis¹⁰ E. Raleigh-Smith^{2,||} D. Rhodes² J. S. Rojo² M. Satrazani¹¹ T. Sauvage¹² C. Shenton^{1,2} C. E. Svensson¹³
 D. Tam⁴ L. Wagner² and D. Yates^{2,14}

¹*School of Mathematics and Physics, University of Surrey, Guildford, GU2 7XH, United Kingdom*

²*TRIUMF, 4004 Wesbrook Mall, Vancouver, British Columbia, V6T 2A3, Canada*

³*School of Physics, Engineering and Technology, University of York, Heslington, York, YO10 5DD, United Kingdom*

⁴*Department of Physics, Simon Fraser University, 8888 University Drive, Burnaby, British Columbia, V5A 1S6, Canada*

⁵*Instituto de Ciencia de Materiales, CSIC Universidad de Sevilla, Avenida Américo Vespucio 49, 41092 Sevilla, Spain*

⁶*Department of Nuclear Engineering, Hanyang University, Seoul, 04763, Republic of Korea*

⁷*Department of Physics and Astronomy, McMaster University, Hamilton, Ontario, L8S 4L8, Canada*

⁸*Institut d'Estudis Espacials de Catalunya, Universitat Politècnica de Catalunya, E-08034 Barcelona, Spain*

⁹*Facility for Rare Isotope Beams, Michigan State University, East Lansing, Michigan 48824, USA*

¹⁰*Institut für Kernphysik, Technische Universität Darmstadt, Schlossgartenstraße 2, Darmstadt D-64289, Germany*

¹¹*Department of Physics, University of Liverpool, Liverpool, L69 7ZE, United Kingdom*

¹²*CEMHTI, UPR3079 CNRS, 1D avenue de la Recherche Scientifique, 45071 Orléans, France*

¹³*Department of Physics, University of Guelph, Guelph, Ontario, N1G 2W1, Canada*

¹⁴*Department of Physics and Astronomy, University of British Columbia, Vancouver, British Columbia, V6T 1Z4, Canada*



(Received 5 September 2024; revised 29 November 2024; accepted 5 February 2025; published 17 March 2025)

This Letter reports on the first cross-section measurements for the $^{94}\text{Sr}(\alpha, n)^{97}\text{Zr}$ and $^{86}\text{Kr}(\alpha, n)^{89}\text{Sr}$ reactions. In particular, our measurement of $^{94}\text{Sr}(\alpha, n)^{97}\text{Zr}$ is the first weak r -process reaction cross section obtained using a radioactive ion beam. This experiment was enabled by the use of novel solid helium targets, comprised of silicon thin films with high helium incorporation obtained via a sputtering technique. Yield measurements were performed at center-of-mass energies of 10.4 and 9.0 MeV for the $^{86}\text{Kr}(\alpha, n)^{89}\text{Sr}$ reaction, and 9.9 MeV for $^{94}\text{Sr}(\alpha, n)^{97}\text{Zr}$, extending into the respective Gamow energy windows for a temperature of 5 GK. Reactions were uniquely identified by prompt γ rays detected in coincidence with heavy ions selected by a recoil mass spectrometer. The obtained cross sections are smaller than predicted for both reactions. In the case of $^{94}\text{Sr}(\alpha, n)^{97}\text{Zr}$, the reaction rate found here is lowered by an order of magnitude at temperatures below 5 GK, which is expected to impact the predicted abundance of ruthenium, a signature weak r -process element.

DOI: [10.1103/PhysRevLett.134.112701](https://doi.org/10.1103/PhysRevLett.134.112701)

Uncovering the emergence of heavy elements beyond iron in the Universe represents a frontier of research at the intersection of nuclear physics, astrophysics, and

astronomy. Approximately half of the elements heavier than iron were formed via the rapid neutron capture process, or r process [1]. However, the precise nature of the r process, or even whether there exist multiple components of the r process, is still a topic of intense ongoing debate [2–4]. Constraining the astrophysical conditions required to drive the r process, and identifying sites where such conditions occur in nature, lies at the heart of this challenge. The gravitational wave event GW170817 [5], followed by its kilonova counterpart [6], provided the first direct evidence that neutron-star mergers (NSMs) can undergo an r process [7,8]. However, NSMs as the dominant r -process site present a number of challenges in reconciling galactic chemical evolution models with

*Contact author: matthew.williams@surrey.ac.uk

[†]Present address: Physics Division, Argonne National Laboratory, Lemont, 60439, Illinois, USA

[‡]Present address: Grand Accélérateur National d'Ions Lourds (GANIL), CEA/DRF-CNRS/IN2P3, F-14076 Caen Cedex 05, France

[§]Present address: Triangle Universities Nuclear Laboratory, Durham, North Carolina 27708, USA

^{||}Present address: Lawrence Livermore National Laboratory, Livermore, California 94550, USA

observations [9,10]. Metal-poor stars provide valuable insight into the r process and early chemical history of our galaxy, preserving the nucleosynthetic fingerprints of only one or a few heavy-element-producing events [11]. While the r -process abundance pattern shows a remarkable degree of robustness, these ancient stars reveal intriguing differentiation in the abundance of elements with $38 \leq Z \leq 47$ in the vicinity of the first r -process peak [12], and also in actinides [13] with respect to the solar r -process abundance pattern. One key step toward solving the r -process puzzle is a better understanding of nucleosynthesis mechanisms that differentiate heavy-element signatures seen in the oldest stars.

A *weak* r -process within the neutrino-driven wind of core-collapse supernovae (ccSNe) or NSMs has been put forward as a primary mechanism to preferentially produce elements in the first r -process peak with respect to heavier elements [14,15]. Here, nucleosynthesis is dominantly influenced by (α, n) reactions on neutron-rich radioactive nuclei located three to five neutrons away from stability in the temperature range of approximately 3 to 5 GK [16]. Reactions involving isotopes of Kr and Sr have been identified as particularly important in determining the final abundance of weak r -process signatures [17,18]. Unfortunately, at present, both the astrophysical conditions within the neutrino-driven wind and relevant nuclear reaction rates are highly uncertain. That being said, it has recently been shown that, by constraining key nuclear reaction rates, it is possible to identify which wind conditions satisfy observed weak r -process abundance signatures [18].

A major barrier toward understanding the weak r process is the complete lack of experimental information on key (α, n) reaction rates involving radioactive nuclei. Specifically, in the absence of experimental data, astrophysical models rely on predictions from Hauser-Feshbach theory [19,20]. These calculations may be unreliable away from stability, with discrepancies of a factor ~ 4 recently reported in the context of supernova nucleosynthesis [21,22]. However, to address this issue experimentally, measurements of reactions on short-lived radioactive isotopes must be carried out in inverse kinematics. This presents significant experimental difficulties for α -induced reactions, due to the inability of helium to form chemical compounds. The traditional approaches of gas targets or helium-implanted metallic foils suffer several key experimental drawbacks. For instance, gas targets require large pumping infrastructure, which limit space for detector systems, while metallic foils are limited to small target densities and exhibit rapid helium loss when exposed to an ion beam.

Here, we establish a novel approach for measuring (α, n) reactions on unstable nuclei by using solid, high-density helium targets. These targets were comprised of nanostructured thin films of amorphous silicon with high helium incorporation through the use of a magnetron-sputtering

technique [23,24]. The newly developed targets, coupled with the unique combination of the TIGRESS γ -ray detector array [25] and EMMA recoil spectrometer [26], allowed for the unambiguous identification of (α, n) reactions. In this Letter, we present the first cross-section measurements of the weak r -process reactions $^{86}\text{Kr}(\alpha, n)^{89}\text{Sr}$ and $^{94}\text{Sr}(\alpha, n)^{97}\text{Zr}$, showcasing the performance capability and robustness of Si:He targets for inverse kinematics (α, n) measurements of importance for astrophysics, in particular using a radioactive ion beam.

The experiment was carried out at the ISAC-II facility of TRIUMF, Canada's national particle accelerator center. Yield measurements of the $^{86}\text{Kr}(\alpha, n)^{89}\text{Sr}$ reaction were performed at bombarding energies of 246.6(1) and 213.1(1) MeV, using a stable beam of ^{86}Kr , at an intensity of $1 \times 10^7 \text{ s}^{-1}$ (generated by the Off-Line Ion-Source facility, OLIS [27]). For the measurement of $^{94}\text{Sr}(\alpha, n)^{97}\text{Zr}$, radioactive ^{94}Sr ($t_{1/2} = 75.3 \text{ s}$) was produced by impinging 500 MeV protons, delivered by the TRIUMF main cyclotron, on a thick UC_x target. Radioactive ^{94}Sr ions were extracted using the TRIUMF resonant ionization laser ion source (TRILIS) [28] before mass selection through a high-resolution magnetic separator. The Charge State Booster (CSB) [29], an electron cyclotron resonance ion source, was then used to charge-breed the ^{94}Sr to 16^+ before subsequent acceleration to an energy of 259.0(1) MeV. This resulted in an average beam intensity of $\sim 6 \times 10^6 \text{ s}^{-1}$ delivered to the experiment.

The ^{86}Kr and ^{94}Sr beams were impinged on Si:He targets with helium contents of 6.15(31) and 7.95(45) $\times 10^{18} \text{ atoms/cm}^2$, respectively. The target thicknesses and composition were determined by proton elastic backscattering at the CEMHTI-Pelletron facility, Orléans, France. Degraded foils of 8 μm -thick aluminum behind each target were used to reduce the energy of outgoing heavy-ion recoils to within the rigidity limits of EMMA. Prompt γ rays resulting from (α, n) reactions were detected using the TIGRESS high-purity germanium (HPGe) array, in coincidence with heavy-ion recoils transmitted to the focal plane of the EMMA recoil mass spectrometer. Detectors at the focal plane of EMMA comprised a position-sensitive parallel grid avalanche counter (PGAC), followed by an ionization chamber and an ion-implanted silicon detector. Only the PGAC signals were used for recoil γ coincidence identification, with an associated 94(1)% detection efficiency from the wire grid transparency. Standard sources of $^{56,60}\text{Co}$, ^{152}Eu , and ^{133}Ba were used to determine the calibration and efficiency of TIGRESS. The transmission efficiency of recoils through EMMA was evaluated using a combination of GEANT4 [30] simulations and a semi-empirical model of the spectrometer's angular and energy/charge acceptances. Specifically, the reaction kinematics, energy loss, and straggling of recoils passing through the target and degrader foil were simulated using GEANT4.

TABLE I. Summary of parameters used to deduce partial cross sections for the $^{86}\text{Kr}(\alpha, n)^{89}\text{Sr}$ and $^{94}\text{Sr}(\alpha, n)^{97}\text{Zr}$ reactions. The effective center-of-mass energy takes into account the energy dependence of each γ -ray production cross section across the target. The integrated luminosity is the product of the total number of beam ions and the areal density of helium target atoms. The detection efficiency is the product of the recoil detection efficiency, charge state fraction, and γ -ray detection efficiency.

Reaction	E_{cm} (MeV)	E_{γ} (keV)	Events	Efficiency (%)	Integrated Luminosity (μb^{-1})	Partial Cross-section (mb)
$^{86}\text{Kr}(\alpha, n)^{89}\text{Sr}$	10.31(5)	1032	168 ± 20	1.11 ± 0.20	$3.48 \pm 0.43_{\text{sys}} \pm 0.25_{\text{stat}}$	$4.35 \pm 0.70_{\text{sys}} \pm 0.59_{\text{stat}}$
	10.47(6)	1473	334 ± 35	0.914 ± 0.095	"	$10.5 \pm 1.7_{\text{sys}} \pm 1.5_{\text{stat}}$
	10.45(6)	2079	238 ± 22	0.740 ± 0.077	"	$9.2 \pm 1.5_{\text{sys}} \pm 1.1_{\text{stat}}$
	9.05(3)	1032	43 ± 7	1.26 ± 0.17	$5.55 \pm 0.43_{\text{sys}} \pm 0.14_{\text{stat}}$	$0.608 \pm 0.093_{\text{sys}} \pm 0.10_{\text{stat}}$
	9.05(4)	1473	58 ± 21	1.05 ± 0.14	"	$1.09 \pm 0.16_{\text{sys}} \pm 0.39_{\text{stat}}$
$^{94}\text{Sr}(\alpha, n)^{97}\text{Zr}$	9.91(5)	407	162 ± 28	1.12 ± 0.28	$8.86 \pm 0.50_{\text{sys}} \pm 0.19_{\text{stat}}$	$1.63 \pm 0.43_{\text{sys}} \pm 0.30_{\text{stat}}$

Then, the resulting momentum distributions of recoils exiting the degrader were passed through an acceptance map of the spectrometer to estimate the proportion of events transmitted to the focal plane. The transmission efficiency for the ^{89}Sr recoils was found to be 89(7)% and 86(9)% for the incoming beam energies of 246.6 MeV and 213.1 MeV, respectively. The ^{97}Zr recoils had a lower transmission efficiency of 49(10)%, since EMMA was tuned to lower than the central recoil energy in order to reduce the scattered beam rate at the focal plane. The 20% relative uncertainty in the transmission efficiency of ^{97}Zr recoils is the dominant systematic error in our measurement of the $^{94}\text{Sr}(\alpha, n)^{97}\text{Zr}$ cross section presented in Table I. The effect of the excited state population of the residual nucleus was accounted for by calculating the transmission for several different recoil excitation energies, corresponding to the mean excitation predicted by TALYSv2.0 [31] (using default input parameters), as well as upper and lower bounds that encompass 68% of the total population distribution. We find that the transport efficiency only weakly depends on the recoil excitation energy, with an associated uncertainty typically less than half of the systematic error related purely to the spectrometer acceptance map. The aforementioned uncertainties in the transmission efficiencies include this contribution from finite recoil excitation energy, which we add in quadrature with the systematic associated with the acceptance map. Finally, the charge-state distribution of a reduced intensity beam of ^{86}Kr was measured and used to infer the charge-state fractions of ^{89}Sr and ^{97}Zr recoils, using the dependence of the equilibrium charge state on Z and energy predicted by the empirical parametrization of Ref. [32]. The ^{89}Sr recoil charge-state fractions were determined to be 20.1(14) ($q = 21^+$) and 21.5(17)% ($q = 20^+$), for the 246.6 and 213.1 MeV incident beam energies, respectively. For the $^{94}\text{Sr}(\alpha, n)^{97}\text{Zr}$ measurement, the ($q = 23^+$) ^{97}Zr recoil charge-state fraction was 21.3(30)%.

The (α, n) reaction cross sections for the emission of known low-lying γ -ray transitions in ^{89}Sr and ^{97}Zr , respectively, were directly obtained from the experiment. Absolute normalization was achieved through measuring

the total integrated luminosity by monitoring the rate of elastically scattered helium, detected by two 150 mm² silicon surface barrier detectors (SSBs), relative to regular Faraday cup readings. The SSBs were mounted at 20° with respect to the beam axis and covered by 20 μm thick Al foils to completely range out any scattered silicon or aluminium, leaving only well-resolved peaks due to scattered helium and hydrogen (assumed to be from water contamination in the target). This allowed degradation of the helium content to be carefully taken into account (this was observed to decrease by a factor ~ 2 after a total of $\sim 3 \times 10^{11}$ incident ions). Once the scattering rate reached approximately a factor 2 below the initial rate, the target holder was manually rotated to expose a fresh spot to the beam. The scattering rate was observed to return to the previous rate on a *pristine* target spot, indicating a uniform helium content. Moreover, the robustness of the targets is underscored by the reproducible trend in the observed scattering rate with beam exposure after each target move. For the measurement of the $^{94}\text{Sr}(\alpha, n)$ reaction, the ^{94}Sr component of the radioactive beam was determined through particle identification at the EMMA focal plane with and without TRILIS laser ionization. This procedure was repeated several times over the course of the experiment to control for any changes in the ^{94}Sr composition, which had a typical measured value of 75(5)%. The remaining 25% of the beam was a mixture of ^{94}Rb and ^{94}Mo . The beam composition was taken into account by scaling the SSB counts by the ^{94}Sr beam fraction. It is important to note that these contaminants do not impact the $^{94}\text{Sr}(\alpha, n)$ measurement due to the unique identification of ^{97}Zr γ decays.

Figure 1 shows the γ -ray spectra obtained in coincidence with heavy-ion recoils from the $^{86}\text{Kr}(\alpha, n)^{89}\text{Sr}$ and $^{94}\text{Sr}(\alpha, n)^{97}\text{Zr}$ reactions, respectively. The characteristic time-of-flight peaks, produced by correlated γ rays and recoils, which are shown in the insets of Fig. 1, are used to discriminate the reactions of interest from the background. The time-random background is higher in the case of $^{94}\text{Sr}(\alpha, n)^{97}\text{Zr}$ due to the decay of radioactive beam ions scattered into the target chamber. Considering the

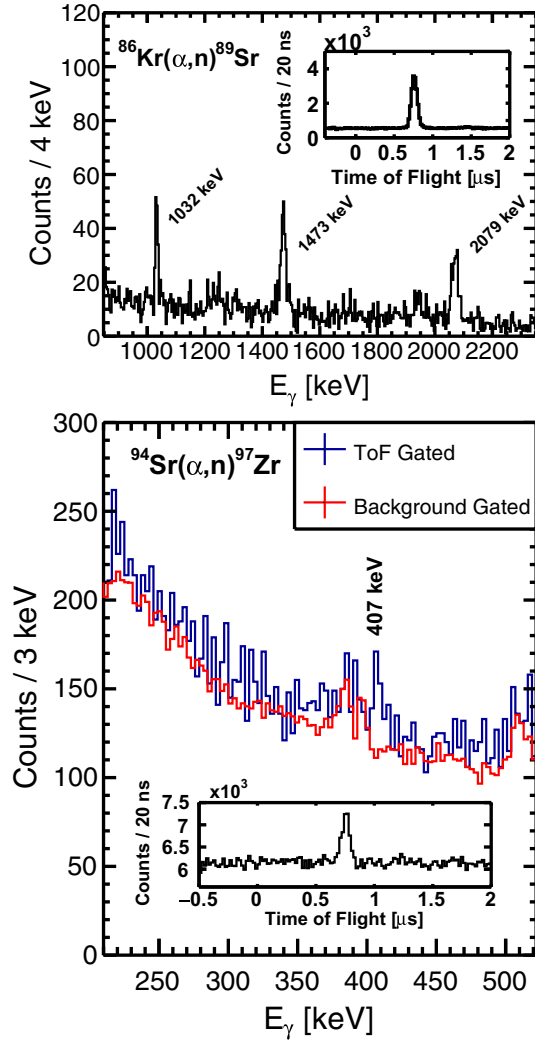


FIG. 1. Coincident γ rays detected from the $^{86}\text{Kr}(\alpha, n)^{89}\text{Sr}$ (top) and $^{94}\text{Sr}(\alpha, n)^{97}\text{Zr}$ (bottom) reactions. The insets display the respective time-of-flight spectra between EMMA and TIGRESS events.

$^{86}\text{Kr}(\alpha, n)^{89}\text{Sr}$ reaction, several strong γ -ray transitions in ^{89}Sr are observed at 1032, 1473, and 2079 keV. This is consistent with reported γ -ray intensities for a prior measurement of the same reaction at higher energies [33], and indeed this is also in line with theoretical calculations, obtained using the TALYS Hauser-Feshbach code [31]. However, at the lowest bombarding energy performed here for the $^{86}\text{Kr}(\alpha, n)^{89}\text{Sr}$ reaction, the transition at 2079 keV is not observed due to limited statistics. In the case of $^{94}\text{Sr}(\alpha, n)^{97}\text{Zr}$, the identification of characteristic transitions in ^{97}Zr presents a significant experimental challenge. In particular, the strongest expected transition in ^{97}Zr (from TALYS calculations) at 1102 keV was obscured by β -delayed background induced by the decay of ^{94}Sr . Moreover, the next-strongest expected transition is associated with the isomeric state at 1264 keV ($t_{1/2} = 102.8$ ns), which is too long-lived to be detected in flight. Fortunately,

the known transition at 407 keV in ^{97}Zr was clearly observed above the background, as displayed in Fig. 1, allowing a partial cross section for the $^{94}\text{Sr}(\alpha, n)^{97}\text{Zr}$ reaction to be measured.

All parameters used to determine partial cross sections for each reaction, pertaining to observed γ -ray transitions, are listed in Table I. The effective center-of-mass energy, $E_{\text{cm}}^{\text{eff}}$, was determined for each transition by solving Eq. (1) for $E_{\text{cm}}^{\text{eff}}$. In this way, the energy loss across the target and energy dependence of the reaction cross section (as predicted by TALYS) is taken into account. The differing energy dependence for each transition leads to slightly different $E_{\text{cm}}^{\text{eff}}$, even for the same incoming and outgoing beam energies, E_i and E_f , respectively:

$$\langle \sigma(E) \rangle = \frac{\int_{E_f}^{E_i} \sigma(E) dE}{\int_{E_f}^{E_i} dE} = \sigma(E_{\text{cm}}^{\text{eff}}). \quad (1)$$

The resulting partial cross sections are compared with predictions from TALYSv2.0 [31] in Figs. 2(a) and 2(b) for $^{86}\text{Kr}(\alpha, n)^{89}\text{Sr}$ and $^{94}\text{Sr}(\alpha, n)^{97}\text{Zr}$, respectively. All measured cross sections are systematically lower than predicted. Furthermore, the observation of characteristic γ rays provides additional information with which to test theoretical calculations. Intriguingly, for the $^{86}\text{Kr}(\alpha, n)^{89}\text{Sr}$ reaction, only the microscopic nuclear-level density (NLD) model of Goriely, Hilaire, and Koning [34] predicts that the 1473 keV γ ray should be populated more than the 2079 keV transition at a center-of-mass energy of ~ 10.4 MeV. Therefore, we adopt this NLD model to compute the central values in the inferred total cross section for both reactions, as opposed to the default phenomenological constant-temperature model.

Considering the comparison between predicted and measured partial cross sections for the $^{86}\text{Kr}(\alpha, n)^{89}\text{Sr}$ reaction further, a global $\sim 60\%$ scaling of the theoretical cross section was found to best fit the experimental data. The same scale factor is found to match the present $^{94}\text{Sr}(\alpha, n)^{97}\text{Zr}$ reaction partial cross section. In order to assess the astrophysical implications of the present Letter, total cross sections were inferred using the predicted fraction of partial to total cross sections from TALYS. For the $^{86}\text{Kr}(\alpha, n)^{89}\text{Sr}$ reaction, we sum the partial cross sections of all observed transitions at a given bombarding energy prior to calculating the predicted fraction of the total reaction cross section. However, since the effective center-of-mass energies for each transition listed in Table I are slightly different for the $E_b = 246.6$ MeV bombarding energy, we first extrapolate the partial cross sections to a common center-of-mass energy of 10.39 MeV. All combinations of α -optical model potentials available in TALYSv2.0 were tested to assess the uncertainty in this extrapolation, which at most extends 80 keV away from the initial effective energy. The scaling of the partial cross sections

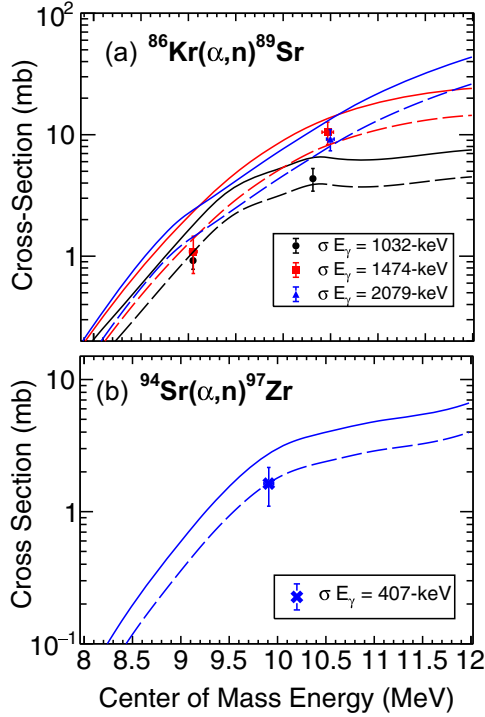


FIG. 2. Partial cross sections for transitions observed from the (a) $^{86}\text{Kr}(\alpha, n)^{89}\text{Sr}$ and (b) $^{94}\text{Sr}(\alpha, n)^{97}\text{Zr}$ reactions. The solid lines indicate predictions from TALYS, with the dashed lines showing the same prediction with a 60% scale factor applied. The TALYS calculations were performed using the default alpha optical potential and γ -ray strength function models, but with the nuclear-level density model of Ref. [34].

amounted to 1.005(13), 0.9578(51), and 0.9323(38) for the 1032, 1473, and 2079 keV transitions, respectively. All available combinations of NLD and γ -ray strength function (γ SF) models in TALYSv2.0 were explored to obtain the fraction of the observed sum of partial cross sections to the inferred total cross section. However, the adopted fraction for the central value is taken from TALYS calculations using the NLD model of Ref. [34] and the default α optical model and γ SF. The uncertainty in the fraction results from the minimum and maximum spread of values from all combinations of γ SF and NLDs. The fractions, associated uncertainty, and inferred total cross sections are listed in Table II, alongside the predicted total cross sections from TALYS with default model inputs.

The maximum relative uncertainty in the calculated partial cross sections as a fraction of the total cross section was found to be $\sim 16\%$ for observed transitions in $^{86}\text{Kr}(\alpha, n)^{89}\text{Sr}$, and 50% for the 407 keV transition in $^{94}\text{Sr}(\alpha, n)^{97}\text{Zr}$, which we conservatively adopt as the model uncertainty for the respective total inferred cross sections. The average scale factor between the experimentally inferred cross section and the theoretical cross section is then found to be $(54 \pm 15)\%$ and $(56 \pm 32)\%$ for the $^{86}\text{Kr}(\alpha, n)^{89}\text{Sr}$ and $^{94}\text{Sr}(\alpha, n)^{97}\text{Zr}$ reactions, respectively,

TABLE II. Summed partial cross sections and inferred total cross sections (σ_{tot}) from this Letter. Predicted values from TALYSv2.0 with default model inputs are also listed alongside the calculated fractions used to infer the total cross section from the partial cross sections. The central values for the fractions are also calculated using default model inputs, except for the NLD, which is adopted from Ref. [34].

Reaction	E_{cm} (MeV)	Measured σ (mb)	Fraction (%)	Inferred σ_{tot} (mb)	Theory σ_{tot} (mb)
$^{86}\text{Kr}(\alpha, n)$	10.39(6)	23.0(41)	46.1(30)	50.0(95)	72.2
	9.05(4)	1.70(48)	28.6(47)	5.9(19)	14.6
$^{94}\text{Sr}(\alpha, n)$	9.91(5)	1.63(51)	$12.3^{+6.1}_{-1.4}$	13.3(78)	23.0

from which we extract the resulting thermonuclear reaction rate using the EXP2RATE code by T. Rauscher [35]. The tabulated rates found in the Appendix are a significant constraint beyond previous sensitivity studies, which sample all (α, n) reaction rates from log-normal distributions spanning factors of 0.1 and 10 [17] and 0.3 and 3 [18], respectively, within $\pm 1\sigma$ confidence limits.

The newly determined rate for the $^{94}\text{Sr}(\alpha, n)^{97}\text{Zr}$ reaction is found to extend from a factor 4 to an order of magnitude below the recommended rate taken from REACLIB [36] at weak r -process temperatures ($3 \leq T \leq 5$ GK). Details of our thermonuclear reaction rates and comparison to REACLIB at weak r -process temperatures can be found in the Appendix. In a recent weak r -process sensitivity study, the $^{94}\text{Sr}(\alpha, n)^{97}\text{Zr}$ reaction rate was found to have a strong positive correlation with the final abundance of Ru, with a correlation factor of ~ 0.5 [17]. Therefore, based on the present Letter, Ru yields from weak r -process models are expected to decrease by up to a factor of ~ 5 . Importantly, Ru is identified as a key marker for weak r -process nucleosynthesis in a large sample of metal-poor stars [37]. Consequently, the reduction in both the overall abundance and associated nuclear uncertainty in Ru, implied by the present Letter, is expected to directly impact the identification of weak r -process enhanced metal-poor stars.

In summary, we have performed the first cross-section measurements of both $^{86}\text{Kr}(\alpha, n)^{89}\text{Sr}$ and $^{94}\text{Sr}(\alpha, n)^{97}\text{Zr}$, which have been identified as important reactions in the context of a weak r process occurring in the neutrino-driven winds of ccSNe and NSMs [17,18]. Our lowest-energy measurements for $^{86}\text{Kr}(\alpha, n)^{89}\text{Sr}$ and $^{94}\text{Sr}(\alpha, n)^{97}\text{Zr}$ are located close to their respective Gamow peaks at $T = 4.6$ GK ($E_{\text{cm}} = 9.1$ MeV) and $T = 5$ GK ($E_{\text{cm}} = 10$ MeV), corresponding to the upper temperature range of weak r -process conditions. Furthermore, in the case of the $^{94}\text{Sr}(\alpha, n)^{97}\text{Zr}$ reaction, this Letter represents the first measurement of a weak r -process reaction on a radioactive nucleus. Our resulting cross sections are found to be approximately a factor 2 below predictions from the

statistical model code TALYSv2.0 [31]. However, the thermonuclear reaction rate for $^{94}\text{Sr}(\alpha, n)^{97}\text{Zr}$, extracted from the present Letter, is an order of magnitude lower at weak r -process temperatures than the evaluated REACLIB rate [36] adopted by the sensitivity study of Bliss *et al.* [17]. Consequently, this is expected to impact predictions for the abundance of Ru, a key weak r -process marker, resulting from ccSNe and NSM nucleosynthesis models. Furthermore, this Letter demonstrates for the first time the feasibility of using novel solid helium targets, formed through a magnetron-sputtering technique, to measure α -induced reactions of importance for astrophysics, including experiments that require beams of short-lived radioactive nuclei, thereby opening new possibilities for similar measurements in the future.

Acknowledgments—The authors acknowledge the generous support of the Natural Sciences and Engineering Research Council of Canada. TRIUMF receives federal funding via a contribution agreement through the National Research Council of Canada. UK authors were supported by the Science and Technologies Facilities Council (STFC). Solid helium target development was supported by Spanish Grant No. PID2021-124439NB-I000 (co-financed by EU FEDER) and the French EMIR&A network for the provision of irradiation beam time at the CEMHTI-Pelletron facility for ion-beam analyses. M. W. acknowledges support from the STFC Ernest Rutherford Fellowship (ST/W00321X/1).

-
- [1] J. J. Cowan, C. Sneden, J. E. Lawler, A. Aprahamian, M. Wiescher, K. Langanke, G. Martínez-Pinedo, and F.-K. Thielemann, *Rev. Mod. Phys.* **93**, 015002 (2021).
- [2] F.-K. Thielemann, A. Arcones, R. Käppeli, M. Liebendörfer, T. Rauscher, C. Winteler, C. Fröhlich, I. Dillmann, T. Fischer, G. Martínez-Pinedo *et al.*, *Prog. Part. Nucl. Phys.* **66**, 346 (2011).
- [3] S. Shibagaki, T. Kajino, G. Mathews, S. Chiba, S. Nishimura, and G. Lorusso, *Astrophys. J.* **816**, 79 (2016).
- [4] Z. Xiong, G. Martínez-Pinedo, O. Just, and A. Sieverding, *Phys. Rev. Lett.* **132**, 192701 (2024).
- [5] B. P. Abbott *et al.* (LIGO Scientific Collaboration and Virgo Collaboration), *Phys. Rev. Lett.* **119**, 161101 (2017).
- [6] M. R. Drout, A. L. Piro, B. Shappee, C. Kilpatrick, J. Simon, C. Contreras, D. Coulter, R. Foley, M. Siebert, N. Morrell *et al.*, *Science* **358**, 1570 (2017).
- [7] D. Watson, C. J. Hansen, J. Selsing, A. Koch, D. B. Malesani, A. C. Andersen, J. P. Fynbo, A. Arcones, A. Bauswein, S. Covino *et al.*, *Nature (London)* **574**, 497 (2019).
- [8] N. Domoto, M. Tanaka, S. Wanajo, and K. Kawaguchi, *Astrophys. J.* **913**, 26 (2021).
- [9] Y.-Z. Qian, *Astrophys. J.* **534**, L67 (2000).
- [10] B. Côté, M. Eichler, A. Arcones, C. J. Hansen, P. Simonetti, A. Frebel, C. L. Fryer, M. Pignatari, M. Reichert, K. Belczynski *et al.*, *Astrophys. J.* **875**, 106 (2019).
- [11] C. M. Sakari, V. M. Placco, E. M. Farrell, I. U. Roederer, G. Wallerstein, T. C. Beers, R. Ezzeddine, A. Frebel, T. Hansen, E. M. Holmbeck *et al.*, *Astrophys. J.* **868**, 110 (2018).
- [12] C. Sneden, J. J. Cowan, and R. Gallino, *Annu. Rev. Astron. Astrophys.* **46**, 241 (2008).
- [13] E. M. Holmbeck, T. M. Sprouse, M. R. Mumpower, N. Vassh, R. Surman, T. C. Beers, and T. Kawano, *Astrophys. J.* **870**, 23 (2019).
- [14] A. Arcones and F. Montes, *Astrophys. J.* **731**, 5 (2011).
- [15] C. Hansen, F. Montes, and A. Arcones, *Astrophys. J.* **797**, 123 (2014).
- [16] J. Bliss, A. Arcones, F. Montes, and J. Pereira, *J. Phys. G* **44**, 054003 (2017).
- [17] J. Bliss, A. Arcones, F. Montes, and J. Pereira, *Phys. Rev. C* **101**, 055807 (2020).
- [18] A. Psaltis, A. Arcones, F. Montes, P. Mohr, C. J. Hansen, M. Jacobi, and H. Schatz, *Astrophys. J.* **935**, 27 (2022).
- [19] T. Rauscher and F.-K. Thielemann, *At. Data Nucl. Data Tables* **75**, 1 (2000).
- [20] T. Rauscher and F.-K. Thielemann, *At. Data Nucl. Data Tables* **79**, 47 (2001).
- [21] M. Williams *et al.*, *Phys. Rev. C* **107**, 035803 (2023).
- [22] G. Lotay, S. Gillespie, M. Williams, T. Rauscher, M. Alcorta, A. Amthor, C. Andreoiu, D. Baal, G. Ball, S. Bhattacharjee *et al.*, *Phys. Rev. Lett.* **127**, 112701 (2021).
- [23] V. Godinho, F. J. Ferrer, B. Fernández, J. Caballero-Hernandez, J. Gomez-Camacho, and A. Fernandez, *ACS Omega* **1**, 1229 (2016).
- [24] B. Lacroix, A. Fernández, N. Pyper, A. J. Thom, and C. T. Whelan, *Appl. Surf. Sci.* **683**, 161772 (2025).
- [25] G. Hackman and C. Svensson, *Hyperfine Interact.* **225**, 241 (2014).
- [26] B. Davids, M. Williams, N. Esker, M. Alcorta, D. Connolly, B. Fulton, K. Hudson, N. Khan, O. Kirsebom, J. Lighthall *et al.*, *Nucl. Instrum. Methods Phys. Res., Sect. A* **930**, 191 (2019).
- [27] K. Jayamanna, F. Ames, G. Cojocar, R. Baartman, P. Bricault, R. Dube, R. Laxdal, M. Marchetto, M. MacDonald, P. Schmor *et al.*, *Rev. Sci. Instrum.* **79**, 02C711, (2008).
- [28] J. Lassen, R. Li, M. Mostamand, A. Gacsbaranyi, P. Kunz, C. Babcock, D. Bishop, A. Teigelhöfer, F. Ames, and A. Gottberg, *Nucl. Instrum. Methods Phys. Res., Sect. B* **541**, 137 (2023).
- [29] J. Adegun, F. Ames, and O. Kester, *J. Phys. Conf. Ser.* **2743**, 012064 (2024).
- [30] S. Agostinelli, J. Allison, K. a. Amako, J. Apostolakis, H. Araujo, P. Arce, M. Asai, D. Axen, S. Banerjee, G. Barrand *et al.*, *Nucl. Instrum. Methods Phys. Res., Sect. A* **506**, 250 (2003).
- [31] A. Koning, S. Hilaire, and S. Goriely, *Eur. Phys. J. A* **59**, 131 (2023).
- [32] K. Shima, T. Ishihara, and T. Mikumo, *Nucl. Instrum. Methods Phys. Res.* **200**, 605 (1982).

- [33] E. Wallander, A. Nilsson, L. Ekström, G. Jones, F. Kearns, T. Morrison, H. Price, P. Twin, R. Wadsworth, and N. Ward, *Nucl. Phys.* **A361**, 387 (1981).
- [34] S. Goriely, S. Hilaire, and A. J. Koning, *Phys. Rev. C* **78**, 064307 (2008).
- [35] T. Rauscher, EXP2RATE v2.1, <http://nucastro.org/codes.html> (2024).
- [36] R. H. Cyburt, A. M. Amthor, R. Ferguson, Z. Meisel, K. Smith, S. Warren, A. Heger, R. Hoffman, T. Rauscher, A. Sakharuk *et al.*, *Astrophys. J. Suppl. Ser.* **189**, 240 (2010).
- [37] C. J. Hansen, A. C. Andersen, and N. Christlieb, *Astron. Astrophys.* **568**, A47 (2014).

End Matter

Appendix—This Appendix provides our tabulated reaction rates for $^{86}\text{Kr}(\alpha, n)^{89}\text{Sr}$ and $^{94}\text{Sr}(\alpha, n)^{97}\text{Zr}$ at weak r -process temperatures. The mean and low rates in Table III were calculated by scaling the inclusive (α, xn) cross sections predicted by TALYSv2.0 [31] with the scale factors of 0.54(14) and 0.56(32) for the $^{86}\text{Kr}(\alpha, n)^{89}\text{Sr}$ and $^{94}\text{Sr}(\alpha, n)^{97}\text{Zr}$ reactions, respectively. Default input models

were assumed for the α OMP and γ SF, but adopting the NLD model of Ref. [34]. However, for the high rate, we only scale the $(\alpha, 1n)$ cross section from TALYS, leaving all other open neutron channels unchanged. The code EXP2RATE [35] was then used to calculate the scaled reaction rates. Literature values taken from the REACLIB database [36] are also listed in Table III for comparison.

TABLE III. Tabulated thermonuclear reaction rates at weak r -process temperatures for the $^{86}\text{Kr}(\alpha, n)^{89}\text{Sr}$ and $^{94}\text{Sr}(\alpha, n)^{97}\text{Zr}$ reactions determined from the present Letter, expressed in units of $\text{cm}^3 \text{mol}^{-1} \text{s}^{-1}$. Rates taken from the REACLIB database [36] are also listed for each reaction.

T (GK)	$N_A \langle \sigma v \rangle ^{86}\text{Kr}(\alpha, n)^{89}\text{Sr}$				$N_A \langle \sigma v \rangle ^{94}\text{Sr}(\alpha, n)^{97}\text{Zr}$			
	REACLIB	Low	Medium	High	REACLIB	Low	Medium	High
3.0	1.60×10^{-5}	4.55×10^{-6}	6.06×10^{-6}	8.06×10^{-6}	1.21×10^{-5}	7.89×10^{-7}	1.84×10^{-6}	2.90×10^{-6}
3.5	5.30×10^{-4}	1.64×10^{-4}	2.18×10^{-4}	2.90×10^{-4}	4.53×10^{-4}	2.98×10^{-5}	6.94×10^{-5}	1.10×10^{-4}
4.0	9.06×10^{-3}	2.98×10^{-3}	3.98×10^{-3}	5.30×10^{-3}	7.71×10^{-3}	5.83×10^{-4}	1.36×10^{-3}	2.16×10^{-3}
4.5	9.46×10^{-2}	3.26×10^{-2}	4.36×10^{-2}	5.83×10^{-2}	7.36×10^{-2}	6.95×10^{-3}	1.62×10^{-2}	2.6×10^{-2}
5.0	6.73×10^{-1}	2.41×10^{-1}	3.24×10^{-1}	4.35×10^{-1}	4.57×10^{-1}	5.60×10^{-2}	1.31×10^{-1}	2.11×10^{-1}